Structure and properties of silver-containing a-C(H) films deposited by plasma immersion ion implantation

J.L. Endrino [a,b,*], R. Escobar Galindo [b], H.-S. Zhang [c], M. Allen [d], R. Gago [b,e], A. Espinosa [b], A. Anders [a]

[a] Plasma Applications Group, Lawrence Berkeley National Laboratory, Berkeley, CA 94720, USA
[b] Instituto de Ciencias de Materiales de Madrid, C.S.I.C., Madrid 28049, Spain
[c] Mechanial Engineering Department, University of California Berkeley, Berkeley, CA 94720, USA
[d] SUNY Upstate Medical University, Syracuse, NY 13210, USA
[e] Centro de Micro-Análisis de Materiales, Universidad Autónoma de Madrid, E-28049, Spain

Abstract

In this study, we have grown silver-containing hydrogenated (a-C:H) and non-hydrogenated (a-C) amorphous carbon coatings by two plasma immersion ion implantation methods: I) chemical vapor deposition of methane combined with pulsed filtered cathodic arc deposition of silver, and II) by alternating arc pulses from graphite and silver in a dual cathodic arc plasma source. This unique "bias selective" feature of the deposition system allowed the deposition of silver with the substrates at ground and avoided the sputtering of the grown a-C film. Chemical composition of the samples was analyzed by acquiring their compositional depth-profiles using radio-frequency Glow Discharge Optical Emission Spectroscopy (rf-GDOES), while the microstructural properties were analyzed by X-ray absorption near edge spectroscopy (XANES) and Raman spectroscopy. In this contribution, we compare mechanical and biomedical properties by means of nanoindentation and cell viability tests, respectively, of a-C(H) films obtained by two different plasma immersion ion implantation techniques.

Keywords: Plasma immersion ion implantation; Amorphous carbon; Silver; X-ray absorption spectroscopy; Raman; Nanoindentation; Cell viability

1. Introduction

Diamond-like carbon (DLC) films are of interest to many applications due to their favorable mechanical and tribological properties [1–4]. They have also generated interest in the biomedical field because of their high biocompatibility and perform well as a surface that will support appropriate cellular activity, [5–13]. Strictly speaking, the term "DLC" includes a broad range of sp^3-rich carbon materials with good tribological properties. In this manuscript, we will use the common notation of a-C:H and a-C to refer to hydrogenated and hydrogen-free DLC deposited by two different plasma immersion implantation and deposition techniques, respectively. Because of their amorphous nature, amorphous carbon films are capable of embedding metallic elements, which can add to their functionality. In recent work, the biocide function of radio-frequency plasma-assisted chemical vapor deposition (RF-PACVD) a-C:H films has been described as they were doped with certain toxic elements such as silver, copper and vanadium deposited using DC (direct current) magnetron sputtering [14], Other studies have pointed out the possibility of incorporating silver into a-C coatings by pulsed laser deposition (PLD) with the use of a silver–graphite composite target [15,16]. In general, the underlying idea of these studies is that by varying the alloy element concentration, it is possible to tailor the composite metal–DLC film to a desired point where the biocidal effect of the metal against microorganisms such as harmful bacteria is maximized yet the biocompatibility is not (yet) jeopardized. Other studies in the deposition of mixed DLC–Ag materials have been carried out by magnetron sputtering combined

* Corresponding author. Plasma Applications Group, Lawrence Berkeley National Laboratory, Berkeley, CA 94720, USA. Tel.: +1 510 486 6081; fax: +1 510 486 4374.
E-mail address: JLEndrino@lbl.gov (J.L. Endrino).

with pulsed laser deposition [17], electron cyclotron resonance DC (ECR-DC) sputtering [18] and thermionic vacuum arc [19].

Composite amorphous carbon/Ag films have also attracted attention with respect to their optical properties, these coatings can be made transparent and have low emissivity which make them attractive for window applications [20].

It has also been suggested that the doping of DLC with conductive metals such as silver may be used as coating materials for electrodes in electrochemical analysis in microelectromechanical systems (MEMS), doped DLC materials may provide a window for a broad range of electrochemical reactions [21].

Independently of the deposition technique of choice, silver and carbon films have contrasting nucleation modes. In a-C or a-C:H films grown by plasma immersion ion implantation and deposition (PIIID), the growth occurs in the sub-surface with energetic ions facilitating the insertion below the surface, and thereby forcing the carbon ions to be closer packed, promoting the formation of sp^3 bonds. On the other hand, silver is known to have a three dimensional (3D) growth, and the minimum thickness for coalescence can strongly depend on the contacting substrate properties [22]. Density functional calculations of the interaction energies of silver adatoms on a graphitic carbon surface have indicated that carbon atoms could be hybridized with silver atoms. Scanning tunneling microscopy (STM) images of silver dimers confirmed this, as images would appear as two distinct atoms on the graphite surface and not as a blurred image of the two [23]. In a-C:H materials, there is the possibility that all dangling bonds of carbon are saturated with hydrogen, and any possible interaction between silver and carbon is consequently minimized. Detailed analysis of the nanostructure of pulsed laser deposited a-C/Ag by use of Z-contrast transmission electron microscopy (Z-TEM) has been reported in a similar study [15]. Such nanostructure was described as arrays of nanocrystalline silver particles embedded in an amorphous carbon matrix with formation of silver clusters as small as 5 nm.

Since clustering during deposition can be one difficulty in the deposition of amorphous carbon–Ag films, processes far from thermodynamic equilibrium, such as PLD [24] and PIIID [25] are in fact good deposition choices of non-hydrogenated a-C–Ag at room temperatures. In contrast, other techniques, which involve higher film condensation temperatures such as RF-PACVD, can result in the loss of a homogeneous nanocomposite profile due to segregation of the metal (silver) to the surface.

In the present work, we have made an exploratory study of the mechanical and biomedical properties of nanocomposite a-C:H–Ag and a-C–Ag coatings prepared using two different hybrid deposition techniques: i) Ag cathodic arc in reactive methane (CH_4) atmosphere and ii) dual-cathode pulsed cathodic arc (PCA) deposition using silver and graphite cathodes. The first of these techniques is a hybrid chemical and physical vapor deposition (CVD/PVD) technique, whereas the latter is a special form of PVD technique.

2. Experimental

Films of a-C:H–Ag and a-C–Ag have been deposited using the dual-cathode arc deposition system shown in Fig. 1. The system contains a dual-cathode "triggerless" mini-gun, which was designed to operate in pulsed mode [26,27]. The two cathodes incorporated in the source were graphite (C1) and silver (C2). The pulsed operation of these cathodes was controlled using a custom National Instruments' LabView™ software. Once the computer has sent a signal to the arc power supply, pulsed arc discharges on individual cathodes are triggered simply by application of a high open circuit voltage (typically 600 V). The plasma stream produced by the source is injected into a 90-degree filter to remove most of the macroparticles, which were formed during the cathodic arc process.

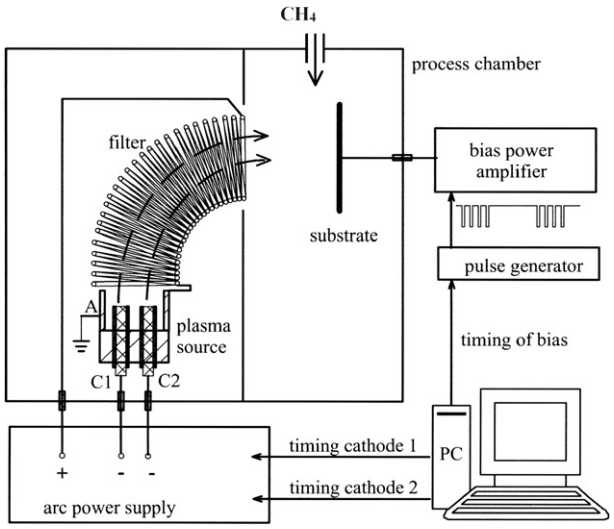

Fig. 1. Schematic of species-selective bias plasma immersion implantation and deposition chamber. The system synchronizes pulsed plasma produced by a dual-cathode "triggerless" mini-gun with pulsed biasing of the substrates. The system is also equipped with a gas inlet port with mass flow controller, which allows for the controlled supply of methane into the chamber.

For the deposition of a-C:H–Ag, carbon and hydrogen are taken from the process gas and silver came from the arc cathode. In the system, the substrates were biased with 1 kV pulses that were 2 μs long, with a duty cycle of 12.5%. Pulsed arcing from the silver cathode occurred simultaneously with the plasma immersion ion implantation and deposition of ions from the methane plasma.

For the deposition of a-C–Ag, the feedstock materials were exclusively the two cathodes; no background gas was needed or added. The residual gas pressure was typically in the 10^{-4} Pa range. One of the advanced features of the system shown in Fig. 1 is that it is equipped with a computer-controlled bias amplifier that can synchronize substrate bias with the pulsed production of plasma. Thus, in order to avoid excessive re-sputtering of carbon atoms during the deposition of the silver, no bias voltage was applied during the deposition of the metallic component, while bias was present when carbon ions arrived [27].

Pure hydrogenated DLC films were initially deposited by CH_4 plasma immersion ion implantation and deposition. In this case, the system was operated in a continuously pulsed bias mode. Methane was supplied into the chamber at a flow rate of 30 sccm. The working pressure was about 9.3 Pa (70 mTorr). Similarly, the silver-containing amorphous hydrogenated film (#2) was

deposited by PIIID using methane and periodically pulsed arcing from a silver cathode. Hydrogen-free films (#3 and #4) were deposited in a vacuum of about 0.67×10^{-3} Pa. Alternate pulses from graphite and silver cathodes were used to manufacture the film with the desired Ag content. The ratio of graphite to silver pulses was 12 to 1. The configurations used in depositing samples #2 and #4 resulted in films with about 5.5 at.% of Ag. All the films were deposited at room temperature and had a thickness of about 100 nm.

Glow Discharge Optical Emission Spectroscopy (GDOES) depth-profile analysis of the deposited films was done using a Jobin Yvon RF GD Profiler equipped with a 4 mm diameter anode. The GDOES was operating at a typical radio-frequency discharge pressure of 650 Pa and power of 40 W. Quantified profiles were obtained automatically using the standard Jobin Yvon QUANTUM Intelligent Quantification software. In order to check for good encapsulation of silver within the samples, thin DLC/Ag/DLC multilayer structures were prepared and analyzed by glow discharge optical emission spectroscopy (GDOES). Also, we have characterized the composition of the samples and monitored the in-depth distribution of H using the high-speed sampling of GDOES.

X-ray absorption near edge structure (XANES) was studied at beamline 7.0 at the Advanced Light Source (ALS) at Lawrence Berkeley National Laboratory. The experiments were performed by measuring the total electron (TEY) and fluorescence (FY) yields. The sp^2 content has been estimated from XANES-TEY by computing the relative ratio of the π^* and σ^* signals. For this purpose, the 282–288 eV and 290–296 eV regions have been considered for the computation of the π^* and σ^* intensity, respectively. The calculation has been normalized to the ratio obtained from an evaporation-deposited a-C film, which is composed of ~95% sp^2 hybrids [28]. Measurements were repeated in 2 different points in each sample in order to confirm the homogeneity of the films.

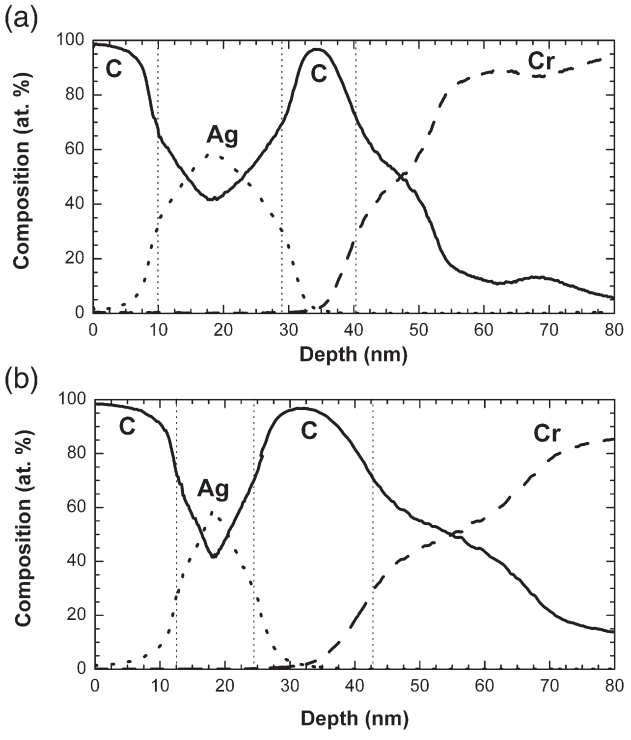

Fig. 2. Compositional GDOES depth-profile of ultrathin DLC/Ag/DLC structures deposited onto Si wafer covered by a sputtered Cr layer (~200 nm thick). DLC layers deposited using: (a) CH_4 PIIID. (b) Filtered cathodic arc.

Table 1
Summary of deposition methods, average silver content determined by glow discharge optical emission spectroscopy (GDOES) and sp^2 content of deposited films

Sample	Material	Deposition DLC	Deposition Ag	Silver (at.%)	$sp^2/(sp^2+sp^3)$
1	a-C:H	CH_4 PIIID	–	0	84
2	a-C:H/Ag	CH_4 PIIID	Filter cathodic arc	5.5±1	84
3	a-C	Filter cathodic arc	–	0	81
4	a-C/Ag	Filter cathodic arc	Filter cathodic arc	5.6±1	82

Raman spectroscopy was used to characterize the microstructure of the carbon films and the changes caused by the silver addition. Raman spectra were acquired with a Jobin Yvon HR 460 monochromator and a nitrogen-cooled CCD (charge coupled device) detector. The excitation light was the 514.5 nm line of an Ar–Kr laser. The incident and scattered beams were focused using an Olympus microscope, and a Kaiser Super-Notch filter was used to suppress the elastically scattered light.

The surface nanomechanical properties of the deposited coatings were studied with a surface force microprobe apparatus (Hysitron Inc.) operated in a controlled temperature of about 25 °C and a relative humidity of about 45%. The shape functions of the diamond tips were determined by a tip calibration procedure involving multiple indentations of a smooth fused quartz samples with 69.9 GPa in-plane modulus. The nanoindentation tests were performed with a diamond tip with 67 nm nominal radius, and both the loading and the unloading time were set to 2 s. The hardness, H, and in-plane elastic modulus, E_r, defined as $E/(1-\nu^2)$, where E and ν are the elastic modulus and Poisson's ratio, respectively, were determined from the recorded load–displacement response in the nanoindentation experiments. The hardness was defined as the maximum load divided by the corresponding indentation area, while the in-plane modulus was calculated from the slope at the initial part of the unloading curves [29].

Cell survival and proliferation were determined using mouse MC3T3 osteoblastic cells that were seeded on coated glass cover slips at an initial density of 5×10^4 cells per disc. The MTT assay was used to quantify the number of viable cells after 3 and 7 days of culture. Data from coated cover slips were normalized to those from uncoated glass control specimens.

3. Results and discussion

3.1. Chemical analyses of a-C:H/Ag and a-C/Ag

We first deposited ultrathin a-C:H/Ag/a-C:H and a-C/Ag/a-C multilayer structures in order to check for the inhibition of Ag migration from a sub-surface layer. Fig. 2 shows the collected GDOES depth-profiles of these two multilayer films. In both cases, the formation of sandwich structures with sharp interfaces

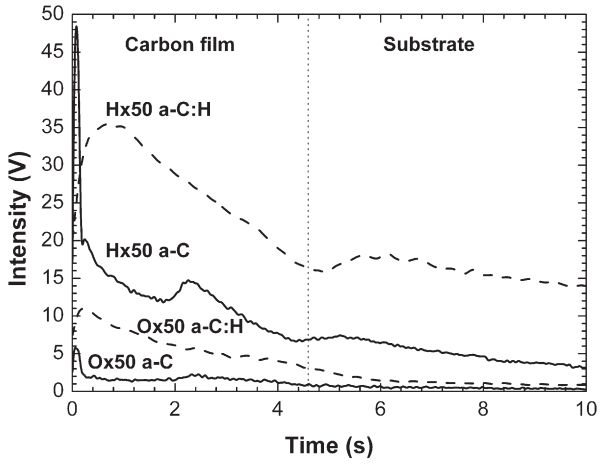

Fig. 3. Intensity of hydrogen and oxygen by glow discharge optical emission spectroscopy (GDOES) for samples #1 (a-C:H) and #3 (a-C) with respect to time.

were observed; silver did not segregate to form a top surface layer. These results served as a positive indication that diamond-like carbon materials deposited under these conditions allow for the incorporation of Ag aggregates within the films.

The results of the quantitative analysis of silver for all the samples are shown in Table 1.

Fig. 3 shows the qualitative depth-profile of the hydrogen and oxygen content of samples #1 (a-C:H) and #3 (a-C). The intensity of the elementary signal is plotted (multiplied by 50) versus the experimental time. The H and O distribution profile across the coating is displayed in only 5 s. The interface between the carbon film and the substrate was located at the time when the substrate signal reached half of its value (not shown in the figure). Although no quantitative information was obtained, it is clear that the hydrogenated sample #1 has higher H and O contents than the a-C sample. The higher presence of oxygen in the hydrogenated sample is likely due to the reduced pumping speed used in order to achieve a higher deposition pressure (about 9.3 Pa) to deposit the a-C:H film using methane gas. The high H signal detected in the substrate of sample #1 could be related to a background increase due to changes in the emission lines because of the hydrogen present in the glow discharge plasma. After subtracting this background, the hydrogen signal remains significantly higher (~2 times) in the a-C:H sample.

3.2. X-ray absorption near edge spectroscopy (XANES)

XANES has been used to quantify the sp^2 content and to obtain information about the bonding structure of the deposited films. Fig. 3a and b shows the TEY and FY spectra at the C (1 s) edge, respectively. The sp^2 content, as derived from both

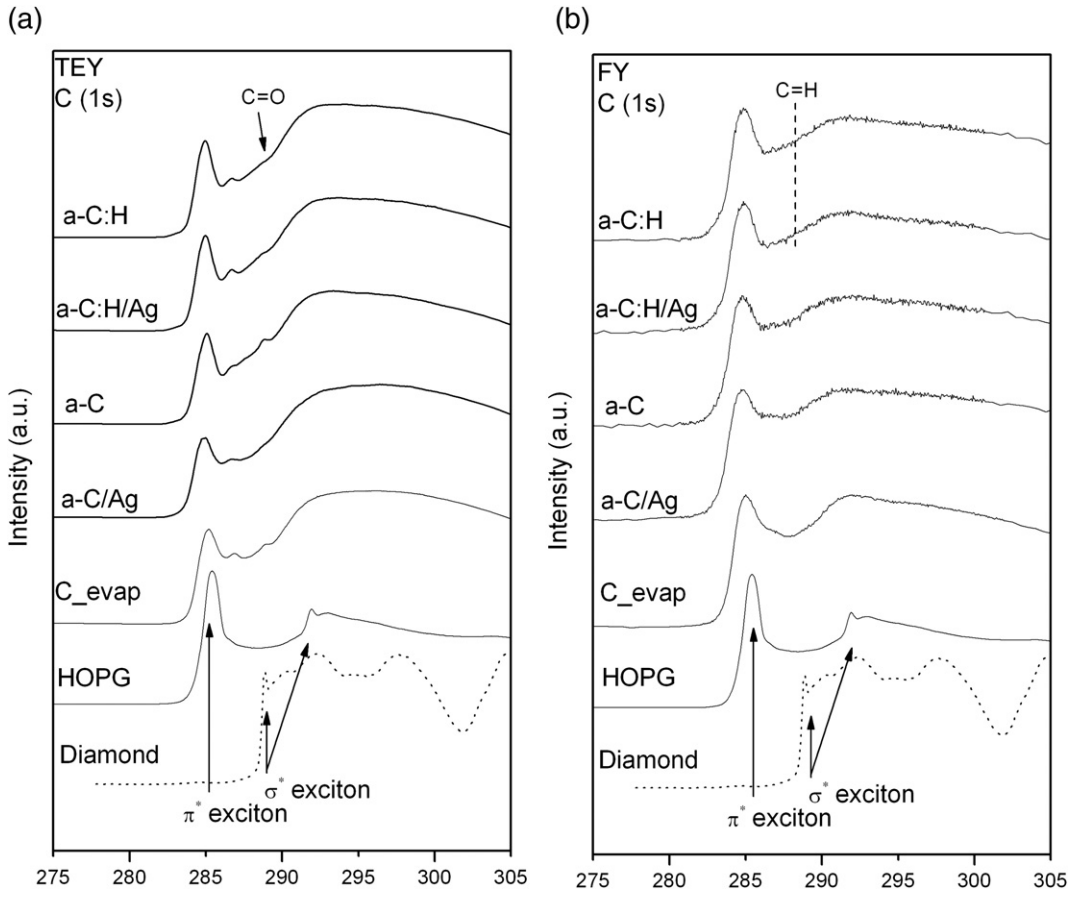

Fig. 4. C K-edge X-ray absorption spectroscopy data for the four deposited silver-free and silver-containing amorphous carbon samples. (a) Total electron yield. (b) Total fluorescence yield.

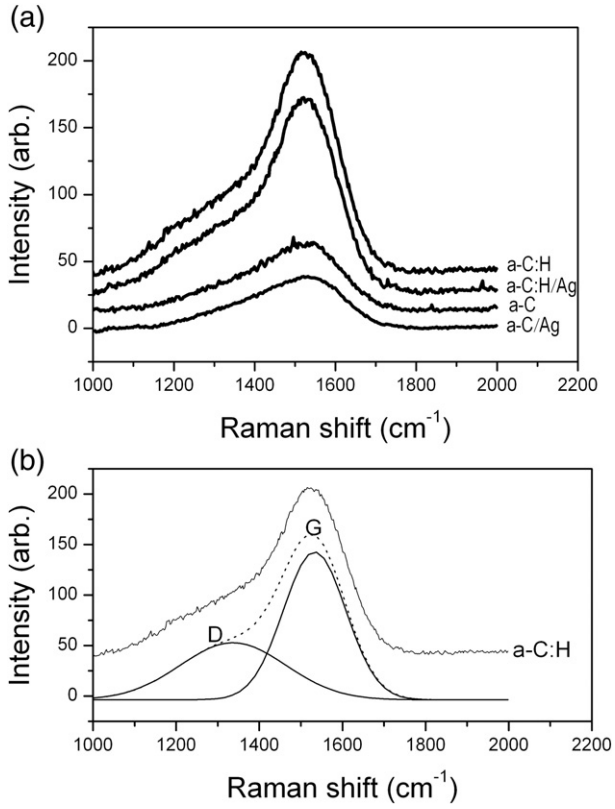

Fig. 5. (a) Raman spectra of all the a-C/Ag and a-C:H/Ag samples. (b) Raman spectrum fitted by Gaussians for sample #1 (a-C:H).

XANES figures, shows that the deposited films have a dominant graphitic character. The increased promotion of sp^3 observed in both figures with respect to evaporated C_evap sample is due to the increased energy of the precursor C flux in the arc set-up, in comparison to the electron beam evaporated films. The TEY (Fig. 4a) shows the presence of a predominant π^* excitation peak at 285.0 eV just slightly lower that the π^* excitation peak for highly oriented pyrolitic graphite (HOPG), which is a signature of disordered in amorphous carbon coatings [28]. The spectra also show the presence of some additional features. There is a small π^* excitation peak at 286.6 eV which is a direct consequence of the redistribution of graphitic bonds near the surface, likely due to the presence of surface contamination. Additionally, there is a very small peak at 288.8 eV which has been reported to correspond to C=O bonds [28]. However none of these features seem to be related to the presence of silver in the films. The calculation of the sp^2 content from the XANES-TEY signal yields a larger value in the case of a-C:H films. This trend is also verified from the XANES-FY signal (Fig. 4b). In Fig. 4b, the spectra from the two a-C:H show a broader σ^* excitation peak in comparison to non-hydrogenated samples, which is due to the presence of C–H states at ~288 eV. Also, the addition of Ag does not affect significantly the bonding structure, both in the case of a-C and a-C:H films. However, a slight decrease in the σ^* excitation peak can be observed in the case of a-C in the TEY and FY spectra.

3.3. Raman spectroscopy

Fig. 5a shows the Raman spectra of the carbon films. The Raman spectra for the hydrogenated samples (#1, #2) have more features than the non-hydrogenated samples (#3, #4). In order to compare among samples, the spectra were fitted using two Gaussians centered at frequencies around 1350 cm^{-1} and 1530 cm^{-1}, commonly named as the D (disorder) and G (graphite) bands [11,30,31]. A typical deconvolution of a Raman spectrum in terms of these two contributions is shown in Fig. 5b for sample #1 after subtracting the background. Table 2 summarizes the fitting parameters, peak positions and full widths at half maximum (FWHM) for all the samples studied. A very useful parameter is the ratio between the intensities of the D and G peaks (I_D/I_G). In many published data, the ratio of the integrated areas under the D and G peaks are presented, but, as recently stated by Casiraghi et al. [30], the area ratio is not the best parameter since it represents the product of the intensity and width ratios, which are better studied separately, as they contain different information. In amorphous carbon, the intensity ratio I_D/I_G is directly related to the size of the sp^2 phase organized in rings and gives an indirect indication of the sp^3 content in the samples. On the other hand, the FWHM of the G peak is sensitive to structural disorder in the film: an increase of the disorder is linked to higher sp^3 content. We can observe how for the hydrogenated carbon film (sample #1) the intensity ratio has a value of 0.42, which is typical of films with a hydrogen content of approximately 20% [30]. Since the addition of silver to the a-C:H (sample #2) did not change neither the intensity ratio nor the FWHM of the G band, the structural disorder of the a-C:H environment does not seem to be dependent in the silver content. The hydrogen-free carbon film (sample #3) has a lower intensity ratio and a wider G peak. In this case, silver inclusion results in a further decrease of the I_D/I_G ratio and a minor broadening of the G peak, this suggests that there is a slight disordering of the a-C environment with silver addition, which could be in part due to the hybridization between carbon and silver and to the energetic condensation of silver ions deposited by filter cathodic arc.

Table 2
Experimental results from Raman spectroscopy of the deposited silver-free and silver-containing amorphous carbon films

Sample no.	Material	D band		G band		I_D/I_G
		Peak (cm^{-1})	FWHM (cm^{-1})	Peak (cm^{-1})	FWHM (cm^{-1})	
1	a-C:H	1354.6±4.6	311.5±6.8	1534.4±0.4	174.4±1.3	0.42±0.01
2	a-C:H/Ag	1352.2±4.6	315.6±5.7	1534.2±0.4	172.1±1.2	0.42±0.01
3	a-C	1351.3±8.7	266.7±9.3	1532.2±2.0	202.5±2.2	0.41±0.03
4	a-C/Ag	1352.0±9.1	228.5±10.4	1535.2±3.0	204.3±3.5	0.40±0.03

Table 3
Summary of nanomechanical properties of silver-free and silver-containing amorphous carbon films deposited by two different plasma immersion ion implantation techniques

Sample	Material	Effective hardness H_{eff} (GPa)	Reduced elastic modulus E_r (GPa)
1	a-C:H	15.7±0.8	85.0±1.7
2	a-C:H/Ag	12.8±0.8	80.4±4.6
3	a-C	21.5±1.6	122.4±8.1
4	a-C/Ag	25.5±0.4	150.9±10.8

3.4. Nanoindentation

Table 3 summarizes the results for nanoindentation tests for all four samples. The mechanical properties of the deposited films varied considerably with respect of the plasma immersion implantation method employed and to some extent with respect to the addition of silver to the amorphous carbon films. The non-hydrogenated films, samples #3 and #4, deposited by the filter cathodic arc technique, have higher effective hardness and reduced elastic modulus than the hydrogenated films, samples #1 and #2. These results correlate well with the XANES data (Fig. 4) since the hydrogenated samples (#1 and #2) had slightly higher amounts of sp^2 hybrids, while the non-hydrogenated amorphous carbon samples (#3 and #4) had slightly higher sp^3 content. The maximum indentation depths and dissipation energies are summarized in Fig. 6; the latter correspond to the areas enclosed inside the indentation curves using a maximum load of 100 μN. Due to the high sp^3 content, a-C has higher hardness and in-plane modulus than a-C:H. With a given indentation load, a-C also has the smaller indentation depth and dissipation energy. The addition of silver deteriorated the mechanical properties of a-C:H, however it did not deteriorate the properties of the a-C film. For silver-containing a-C:H, the addition of silver contributed to softening. In contrast, the addition of silver to a-C films rather increased the coating hardness. This behavior of soft metals playing a role as strengthening dopants has also been reported in the past in other systems including TiC/Ag and TiN/Ag and Mo_2N/Ag [21,32–34]. According to the literature, the embedded nanoparticles of silver in an amorphous matrix could form a heterogeneous structure and decrease the plastic flow. In the current case, this strengthening mechanism could be in part explained by a slight decrease in sp^2 hybrids with the incorporation of silver and by the possibility of increased hybridization between carbon–silver in non-hydrogenated films. Fig. 7 shows that the hardness and in-plane modulus change with tip displacement in the sample. These plots include depth-related mechanical properties of all coating samples. As a general observation, the hardness increases at first with displacement, and then decreases after passing a maximum point. The initial hardness increase was due to the pressure build-up under the tip when elasticity took the majority of deformation under small loads. For large loads, the hardness values become subject to the substrate properties, therefore the curves went down due to the increased contribution from the chromium interface layer. The maximum point of each hardness curve is defined as the effective hardness, H_{eff}, which is a measure of the plastic flow strength of the whole sample [29]. In the case of hydrogenated coatings, is about 20 nm deep for both silver-containing and silver-free samples. However, in the case of the non-hydrogenated films, H_{eff} is located several nanometers deeper for a-C than in the case of the a-C/Ag film. This implies that the addition of silver did not result in a soft mixed carbon and silver sub-surface layer, on the contrary, it

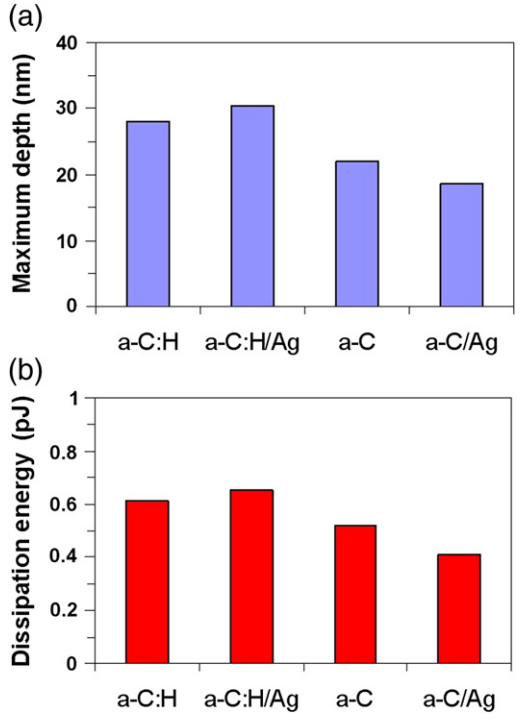

Fig. 6. The maximum indentation depth and dissipation energy for samples #1–#4 using a maximum load of 100 μN.

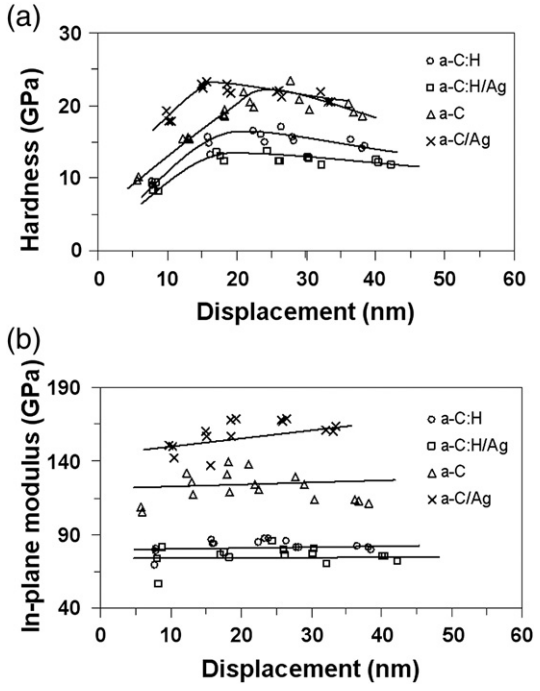

Fig. 7. Plot of nanoindentation tests showing (a) the hardness and (b) in-plane-modulus with respect to indentation displacement for all samples.

seems to have a strengthening effect in the subplantation mechanism of carbon ions. The in-plane modulus of hydrogenated films as well as of non-hydrogenated films are shown in Fig. 7b. The in-plane modulus values were hardly affected by the indentation displacement. However, there are substantial differences in the average value of the in-plane modulus between the two non-hydrogenated films. The highest average in-plane modulus of all samples was obtained for the silver-containing a-C sample (~160 GPa) followed by the silver-free a-C sample (~120 GPa), which is in good correlation with the reduced values for the dissipated energy of indentation shown in Fig. 6.

3.5. Cell viability

The results for cell proliferation with respect to plastic control specimens for all the deposited samples are shown in Fig. 8. Although, in general, it can be observed that hydrogen-free films resulted in an increased cell viability compared to hydrogenated carbon films, statistical analyses on the cell culture data performed by means of paired *t*-test show that after 3 days of culture, viable cell numbers on sample #3 (a-C) are greater than on a-C:H [probability value (*p*-value) of obtaining a similar result <0.01], however, after 7 days of culture there was no statistical difference between the a-C and a-C:H samples. This suggests that although both types of amorphous carbon can be considered biocompatible *in vitro*, a-C is more favorable in the initial adhesion and proliferation of MC3T3 cells. Cell viability test also show that while there was no statistically significant effect of doping with silver for a-C:H coatings, the incorporation of silver had a small initial negative effect (p-value<0.05) at 3 days however this effect was gone by 7 days of culture. The superior cell attachment of mouse osteoblastic cells exhibited by sample #4 (a-C–Ag) after 7 days of culture is a good indicator that this film can also exhibit good osseointegration properties.

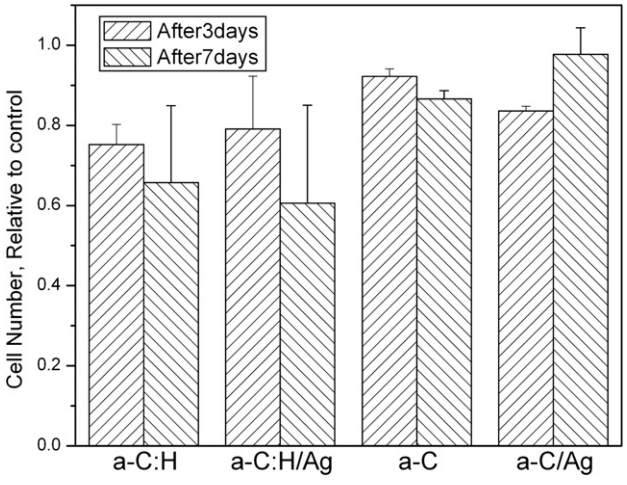

Fig. 8. Effects of coating composition on cell viability *in vitro*. At each time point, data from coated substrates were normalized to those from the uncoated glass control substrate. Viable cell numbers were initially higher on a-C coatings than on a-C:H coatings ($p<0.01$). Incorporation of silver had an early negative effect on the growth of cells on a-C films but by 7 days coatings of all types were covered with a confluent monolayer, indicating their biocompatibility *in vitro*.

The effects of silver addition on the biocidity of doped a-C and a-C:H films is a subject for future work.

4. Summary and conclusions

Coatings of a-C/Ag and a-C:H/Ag have been deposited by two different plasma immersion implantation and deposition techniques and characterized by several chemical and structural techniques including GDOES, XANES, and Raman spectroscopy. Additionally, set of nanomechanical depth-sensing indentation tests and cell proliferation tests have been carried out in order to compare mechanical and biomedical properties of the deposited films.

The compositional profiles obtained by rf-GDOES were used not only to quantify the amount of silver in the samples but also to have a qualitative comparison of the hydrogen in the samples. The results illustrate the importance of the rf-GDOES technique in the collection of rapid compositional profiles to compare different types of amorphous carbon films.

XANES was used to quantify the sp^2 content and to obtain information about the bonding structure within the films and the near-surface. The a-C/Ag film had the lowest amount of sp^2 bonds showing that the species-selective bias technique used in the pulsed filtered cathodic arc deposition lead to high quality silver doped a-C films. Raman spectroscopy confirmed that silver incorporation did not significantly change the short-range environment of a-C and a-C:H films.

Nanoindentation tests showed that hydrogen-free films have higher hardness and in-plane modulus than hydrogenated films, this data correlated well with sp^2 content measurements and structural observations carried out using Raman spectroscopy.

Cell proliferation tests showed that all deposited amorphous carbon films had no cytotoxicity. The highest cell attachment was exhibited by the silver-containing non-hydrogenated a-C sample after a seven-day incubation period.

In summary, non-hydrogenated samples had higher hardness and elastic modulus than hydrogenated ones and they also exhibited superior cell viability of MC3T3 mouse osteoblastic cells. This indicates that they are potential candidates for orthopedic osseointegration applications.

Acknowledgments

The authors acknowledge helpful conversations with Prof. J. M. Albella, Dr. A. de Andrés and Prof. K Komvopoulos. We would also like to thank J. Andersson for his assistance in the collection of XANES spectra. Financial support from the Marie Curie Outgoing Fellowship Grant MOIF-CT-2005-02195 is also gratefully acknowledged. Work at Lawrence Berkeley National Laboratory was supported by the U.S. Department of Energy under Contract No. DE-AC02-05CH11231.

References

[1] E. Alakoski, M. Kiuru, V.-M. Tiainen, A. Anttila, Diamond Relat. Mater. 12 (2003) 2115.
[2] R. Hauert, U. Muller, Diamond Relat. Mater. 12 (2003) 171.

[3] Y.X. Leng, J.Y. Chen, P. Yang, H. Sun, G.J. Wan, N. Huang, Surf. Sci. 531 (2003) 177.
[4] W. Lu, K. Komvopoulos, J. Tribol. Trans. Asme 123 (2001) 641.
[5] M. Allen, F. Law, N. Rushton, Clin. Mater. 17 (1994) 1.
[6] R. Butter, M. Allen, L. Chandra, A.H. Lettington, N. Rushton, Diamond Relat. Mater. 4 (1995) 857.
[7] L. Chandra, M. Allen, R. Butter, N. Rushton, I.M. Hutchings, T.W. Clyne, Diamond Relat. Mater. 5 (1996) 410.
[8] L. Chandra, M. Allen, R. Butter, N. Rushton, A.H. Lettington, T.W. Clyne, Diamond Relat. Mater. 4 (1995) 852.
[9] G. Dearnaley, Clin. Mater. 12 (1993) 237.
[10] G. Dearnaley, J.H. Arps, Surf. Coat. Technol. 200 (2005) 2518.
[11] J. Robertson, Mater. Sci. Eng. R Rep. 37 (2002) 129.
[12] P. Yang, J.Y. Chen, Y.X. Leng, H. Sun, N. Huang, P.K. Chu, Surf. Coat. Technol. 186 (2004) 125.
[13] P. Yang, N. Huang, Y.X. Leng, J.Y. Chen, R.K.Y. Fu, S.C.H. Kwok, Y. Leng, P.K. Chu, Biomaterials 24 (2003) 2821.
[14] R. Hauert, Diamond Relat. Mater. 12 (2003) 583.
[15] M.L. Morrison, R.A. Buchanan, P.K. Liaw, C.J. Berry, R.L. Brigmon, L. Riester, H. Abernathy, C. Jin, R.J. Narayan, Diamond Relat. Mater. 15 (2006) 138.
[16] R.J. Narayan, Diamond Relat. Mater. 14 (2005) 1319.
[17] J.L. Endrino, J.J. Nainaparampil, J.E. Krzanowski, Surface Engineering 2001 — Fundamentals and Applications. Symposium (Mater. Res. Soc. Symposium Proceedings Vol. 697). Mater. Res. Soc. 2002273.
[18] C.P. Lungu, Surf. Coat. Technol. 200 (2005) 198.
[19] C.P. Lungu, I. Mustata, G. Musa, V. Zaroschi, A. Mihaela Lungu, K. Iwasaki, Vacuum 76 (2004) 127.
[20] K. Chiba, T. Takahashi, T. Kageyama, H. Oda, Appl. Surf. Sci. 246 (2005) 48.
[21] J.G. Han, H.S. Myung, H.M. Lee, L.R. Shaginyan, Surf. Coat. Technol. 174–175 (2003) 738.
[22] A. Anders, E. Byon, D.-H. Kim, K. Fukuda, S.H.N. Lim, Solid State Commun. 140 (2006) 225.
[23] D.M. Duffy, J.A. Blackman, Surf. Sci. 415 (1998) L1016.
[24] D.B. Chrisey, G.K. Hubler, Pulsed Laser Deposition of Thin Films, Wiley, New York, 1994.
[25] A. Anders, Handbook of Plasma Immersion Ion Implantation and Deposition, Wiley, New York, 2000.
[26] A. Anders, I.G. Brown, R.A. MacGill, M.R. Dickinson, J. Phys. D Appl. Phys. 31 (1998) 584.
[27] A. Anders, N. Pasaja, S. Sansongsiri, Rev. Sci. Instrum. 78 (2007) 063901.
[28] R. Gago, I. Jimenez, J.M. Albella, A. Climent-Font, D. Caceres, I. Vergara, J.C. Banks, B.L. Doyle, L.J. Terminello, J. Appl. Phys. 87 (2000) 8174.
[29] M.F. Doerner, W.D. Nix, J. Mater. Res. 1 (1986) 601.
[30] C. Casiraghi, A.C. Ferrari, J. Robertson, Phys. Rev. B Condens. Matter Mater. Phys. 72 (2005) 085401.
[31] A.C. Ferrari, J. Robertson, Phys. Rev. B Condens. Matter Mater. Phys. 61 (2000) 14095.
[32] W. Gulbinski, T. Suszko, Surf. Coat. Technol. 201 (2006) 1469.
[33] J.L. Endrino, J.J. Nainaparampil, J.E. Krzanowski, Scr. Mater. 47 (2002) 613.
[34] J.L. Endrino, J.J. Nainaparampil, J.E. Krzanowski, Surf. Coat. Technol. 157 (2002) 95.